

# Probing heavy scalars with an effective $Hb\bar{b}g$ coupling at the LHC

Katri Huitu,<sup>1,\*</sup> Subhadeep Mondal,<sup>1,†</sup> and Biswarup Mukhopadhyaya<sup>2,‡</sup>

<sup>1</sup>*Department of Physics, and Helsinki Institute of Physics,  
P. O. Box 64, FI-00014 University of Helsinki, Finland*

<sup>2</sup>*Department of Physical Sciences, Indian Institute of Science Education and Research,  
Kolkata, Mohanpur 741246, Nadia, West Bengal, India*

We have explored the prospect of probing a neutral scalar ( $H$ ) produced in association with one  $b$ -quark and decaying either invisibly or into a pair of  $b$ -quarks at the LHC with centre of mass energy  $\sqrt{s} = 14$  TeV. In this regard, we adopt an effective theory approach to parameterize a  $Hb\bar{b}g$  vertex arising from a dimension six operator that encompasses the effect of some new physics setting in at a high scale. We concentrate solely on the five-flavor scheme to ascertain the sensitivity of the 14 TeV LHC in probing such an effective coupling as a function of the scalar mass at the highest possible projected luminosity,  $3000 \text{ fb}^{-1}$ . Through our multivariate analysis using machine learning algorithm we show that staying within the perturbative limit of the Wilson coefficient of the effective interaction, evidence with statistical significance of  $3\sigma$  can be obtained in two different signal regions for  $m_H \lesssim 2$  TeV and the scale of new physics  $\Lambda = 3$  TeV.

## I. INTRODUCTION

In the quest for new physics beyond the standard model (BSM) heavy scalar search holds a particular importance. A bunch of new physics models predict an extended scalar sector compared to the SM. In the absence of any direct hint of such non-standard scalar particles, one can only exclude certain regions of parameter space from the experimental data [1–8]. Indirect bounds on these particle masses and their couplings can also be derived from precision electroweak data, see e.g. [9]. Under these circumstances, lack of clarity regarding specific new physics models has aroused considerable interest in effective theories [10–12]. One can parameterize effects of new physics theories through masses and couplings of the particle in consideration. The results derived this way are model independent, and applicable to any new physics theory that can give rise to similar phenomenology.

The  $b$ -quark distribution in the proton is non-negligible at the Large Hadron Collider (LHC). However, its role in the production of the 125 GeV scalar is not estimated to be very significant. On the other hand, with the ever-alive interest in an extended electroweak symmetry breaking sector, it is important to see if any heavier, additional neutral spinless particle can have enhanced production rate due to its  $b$ -coupling. In two Higgs doublet models (2HDM), for example, this is possible for appropriate values of  $\tan\beta$ , the ratio of the two doublet vacuum expectation values (vev) and  $\alpha$ , the doublet mixing angle. One may integrate this idea into a model-independent approach, and see if enhanced production rates follow in terms of some suitably parameterized interaction with a  $b$ -quark pair. This may yield new search channels for additional scalars, and also lead to constraints of the corresponding interactions and scalar masses.

In this paper we look at a non-standard scalar particle ( $H$ ) and its effective coupling to a pair of bottom quarks and a gluon generated through a dimension six effective operator [11]. The considered vertex can give rise to a possible production mode for the heavy scalar with non-negligible cross-section. Experimental collaborations have studied the production of a heavy scalar associated with bottom quarks to look for direct evidence of the scalar decaying into  $b\bar{b}$  resulting in a multi  $b$ -jet final state [13, 14]. Such a computation requires careful inspection of both the four flavor and five flavor schemes [15]. In the conventional four flavor scheme, the relevant production mode  $pp \rightarrow b\bar{b}H$  is either quark or gluon initiated, whereas,  $pp \rightarrow bH$  can also contribute to the same final state. The second production mode can only be obtained in a five-flavor scheme, since it is a bottom quark-gluon initiated process.

Here we only concentrate on the five flavor scheme through a quark-quark-scalar-gluon effective vertex in order to ascertain how significant this contribution can be in probing a heavy scalar. The aforementioned experimental studies [13, 14] rely heavily on a large  $Hb\bar{b}$  coupling. In the context of two Higgs doublet models this is a possibility in the alignment limit of  $\cos(\beta - \alpha) \simeq 0$  [16]. In this limit, decay of the heavy scalar into the gauge bosons are suppressed and thus the LHC search of such a scalar heavily rely on its coupling to the third-generation fermions. In addition, if the  $Hb\bar{b}$  coupling also is too small due to the presence of some new physics one would naturally expect the event rate into multi  $b$ -jet final state to go down. We, therefore, explore a scenario, where the cross-section  $bg \rightarrow bH$  is mostly driven by the effective interaction which does not necessarily have to be small even if the  $Hb\bar{b}$  coupling is small. Thus, in addition to probing the new effective interaction, one can also expect to improve the sensitivity of the  $Hb\bar{b}$  coupling measurement. Once produced, we assume that  $H$  can only decay through two possible decay modes, namely  $b\bar{b}$  and  $\chi\chi$ , where  $\chi$  represents some invisible particle like dark matter. The reason for concentrating only on these channels

\* katri.huitu@helsinki.fi

† subhadeep.mondal@helsinki.fi

‡ biswarup@iiserkol.ac.in

is that, in a sense, they correspond to the ‘difficult situations’ in (heavy) Higgs identification at the two extremes. While a proliferation of  $b$ -jets in the final state threatens the event rate due to suppression via identification efficiencies, one or two  $b$ ’s with missing transverse energy ( $\cancel{E}_T$ ) tends to get swamped by backgrounds. Thus,  $H$  decaying invisibly leaves us with few options to probe. Vector boson fusion production channel cross-section can be small, for example in the alignment limit in 2HDM, which requires one to explore new possibilities. On the other hand,  $H \rightarrow b\bar{b}$  is anticipated to be one of the most prominent decay modes of  $H$  and also the corresponding coupling has significant impact on the production cross-section of  $H$  in five flavor scheme.

In the four flavor scheme, the bottom quark mass ( $m_b$ ) dependence is retained, while in five flavor scheme the  $b$ -quark is treated as a massless parton. Hence in the four flavor scheme, the bottom quark cannot appear as an initial state parton and can only arise from gluon splitting. The non-zero mass protects the gluon splittings from collinear divergences. In the five flavor scheme the computation of higher order correction to the strong coupling constant is simpler, since all the quarks are considered massless. Efforts have been going on in theoretical frontier to match these two schemes [17–21]. The cross-section computed in the four flavor and five flavor schemes are more accurate in the limit  $\frac{\mu}{m_b} \sim 1$  and  $\frac{\mu}{m_b} \gg 1$ , respectively, where  $\mu$  represents the factorization and renormalisation scale [17, 20, 22]. Since in this work we take the new physics scale to be 3 TeV and beyond, we stick to the five flavor scheme only. A novel aspect of the production mode explored here,  $bg \rightarrow bH$ , is that the  $H$  is expected to have a large transverse momentum [23]. Such a scenario can be easily identified as a possible new physics signal.

Over the last decade or so, the LHC analyses have slowly but surely been moving towards the use of machine learning methods to collect and analyze the large data samples [24]. Algorithms like gradient boosted decision trees (BDTs) [25, 26] were used prior to the LHC experiment as well, see e.g. [27]. Machine learning algorithms were highly useful in the discovery of the 125 GeV Higgs boson [28, 29] and subsequently with the accumulation of more and more data - analyzing them requires the use of machine learning algorithms more than ever. The BDT algorithms have widespread application in data analysis and can be used effectively in the context of collider physics to identify new physics signal events depending on the choices of suitable kinematic variables [30]. In this work we have adopted this technique and used the XGBoost toolkit [31].

The paper is organized in the following way. In section II we briefly discuss the theoretical premise of our analysis and the impact of the existing experimental constraints. In section III we introduce the two different signal regions that we have studied in the context of LHC. We discuss in some detail the choice of our kinematic variables for the multivariate analyses. We also high-

light the advantage of such analyses over the canonical cut-based approach. In section III.1 we discuss the impact of our analyses via some chosen benchmark points and subsequently in section III.2 we predict the highest achievable sensitivity of the 14 TeV LHC in probing the present scenario. Finally, in section IV we summarize our work and draw conclusions.

## II. THEORY FRAMEWORK AND CONSTRAINTS

As already mentioned, in this work we maintain a model independent approach. We parameterize the  $Hb\bar{b}g$  vertex in terms of Wilson coefficient that encapsulates the effect of high scale theory. Here  $H$  represents a heavy BSM scalar. The interaction term follows from dimension six  $SU(2) \times U(1)$  gauge invariant operator consistent with the assumption that its origin lies above the electroweak symmetry breaking scale. The effective interaction relevant to our study is  $\frac{f}{\Lambda^2} \bar{b} \sigma^{\mu\nu} b \frac{\lambda_a}{2} G_{\mu\nu}^a H$ , where  $f$  is the Wilson coefficient,  $\Lambda$  represents the cut-off scale at which the new physics sets in,  $\lambda_a$  represents the Gell-Mann matrices,  $\frac{\lambda_a}{2}$  being the  $SU(3)$  generators, and  $G_{\mu\nu}$  is the  $SU(3)$  field strength tensor. Such an interaction can follow from a dimension six operator of the form [11]:

$$\mathcal{O} = \frac{1}{\Lambda^2} (\bar{q} \sigma^{\mu\nu} d) \frac{\lambda_a}{2} G_{\mu\nu}^a \Phi + \text{h.c.}$$

Here  $\Phi$ ,  $q$  and  $d$  represent the new scalar, left handed quark doublet and right handed quark, respectively.

Our objective is to probe the process  $bg \rightarrow bH$  in the context of LHC in the five flavor scheme. A  $Hb\bar{b}$  vertex can lead to similar phenomenology. The two possible production channels are shown in Fig. 1. We explore the

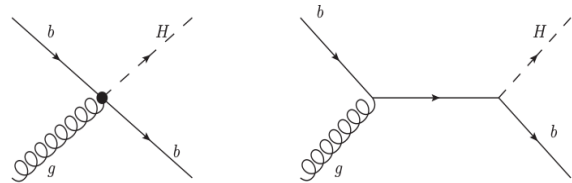


FIG. 1. Possible production modes for  $bg \rightarrow bH$  in presence of the dimension six operator and a  $Hb\bar{b}$  coupling.

possibility of  $H$  either decaying into a pair of  $b$ -quarks or completely invisibly, e.g. into a pair of dark matter particles ( $\chi$ ). Maintaining a model independent approach, we do not assume any specific coupling strengths for these two interactions. Instead we take the branching ratio,  $\text{BR}(H \rightarrow \chi\chi)$ , as a free parameter, which automatically fixes  $\text{BR}(H \rightarrow b\bar{b})$ , since we assume there are no additional decay modes. The other relevant free parameters for our study are  $f$ ,  $\Lambda$ ,  $m_H$  and  $m_\chi$ . The  $H \rightarrow b\bar{b}$  coupling strength determines the contribution of the s-channel mediated diagram in Fig. 1 to the total cross-section and

thus is also a relevant parameter when this cross-section becomes comparable to or dominant over the effective interaction diagram.

Phenomenological constraints on the mass and couplings of such a scalar can be derived from the existing direct search experimental analyses by the ATLAS and CMS Collaborations. However, they are subjected to its production cross-section and existing decay modes. Search for a BSM scalar usually involves the heavy scalar decaying into a pair of SM Higgs which eventually decay into various final states, like four b-jets [1–3], two b-jets along with photons [4, 5], pair of taus [6], or charged leptons and missing energy [7]. The exclusion limit on the masses of such a scalar, therefore, depends upon its single production cross-section, e.g. through gluon fusion, and its coupling to a pair of SM Higgs bosons. These constraints are, thus, not directly applicable to the present scenario. Production of scalars via bottom quark fusion has been studied in [13, 14]. These constraints are again subjected to the  $Hb\bar{b}$  coupling strength. In this work, we assume this coupling to be orders of magnitude smaller compared to what is considered in these experimental studies, which ensures that we are well below the exclusion line throughout the range of  $m_H$ .

The most effective way to a direct search of invisible decay of a scalar is through a vector boson fusion production channel. A BSM scalar can be probed up to 3 TeV with the analyzed data so far [8]. However, this involves the scalar coupling to a pair of gauge bosons. In our present scenario, for simplicity, we assume this coupling to be very weak and as a result such constraints are irrelevant.

### III. COLLIDER STUDY: A MULTIVARIATE ANALYSIS

In this section, we study the collider physics implication of the present scenario. As already discussed, we focus on two possible decay modes of the heavy scalar, namely,  $H \rightarrow \chi\chi$  and  $H \rightarrow b\bar{b}$ . For simplicity, we assume that these are the only two possible decay modes of  $H$ . As a result, the production channel  $b\bar{g} \rightarrow bH$  may lead to two possible signal regions, 1 b-jet +  $\cancel{E}_T$  (SR1) and 3 b-jets (SR2). We explore both these final states in the context of 14 TeV LHC. For this, we perform a multivariate analysis with machine learning technique known as the BDT. For our analysis, we have taken 1000 estimators, maximum depth 4 and learning rate 0.01. We combine data corresponding to chosen kinematic variables for our signal events as well as all the background events from different channels to prepare one single data file. The background events are combined after properly weighting them according to their cross-sections and it has been ensured that there are enough signal events to match the total weight of all the background events. We take 80% of our combined data for training and 20% for testing purpose.

We have used Madgraph5 [32, 33] for parton level event generation and PYTHIA8 [34, 35] for subsequent showering and hadronisation. For the simulation, we use the NNPDF parton distribution function [36, 37]. We have used a dynamic factorisation and renormalisation scale. For a single heavy particle production it is simply  $m^2 + p_T^2$ , where,  $m$  and  $p_T$  represent the mass and transverse momentum of the particle. For production of a pair of heavy particles it is the geometric mean of  $m^2 + p_T^2$  for each particle [44]. Detector simulation was performed using Delphes3 [38–40]. Jets were constructed in FastJet [41] following anti-kt algorithm [42]. Appropriate  $b$ -jet tagging and mistagging efficiencies have been implemented within the Delphes platform following recommended values by the ATLAS Collaboration [43]. Throughout this study, we have used next-to-leading order (NLO) cross-sections for all the SM processes [33]. For the signal we assume that any new physics effect including the NLO contribution is clubbed with the Wilson coefficient of the dimension six operator.

#### Signal Region 1: 1 b-jet + $\cancel{E}_T$

In this signal region  $H$  decays invisibly, resulting in the sole  $b$ -jet associated with a large transverse missing energy. We put the following criteria to select events in this signal region: the final state should have only one  $b$ -jet with  $p_T^b > 120$  GeV and  $|\eta^j| < 2.5$ , at least two light jets with  $p_T^j > 40$  GeV and  $|\eta^j| < 2.5$ , no charged leptons with  $p_T^\ell > 10$  GeV and  $|\eta^\ell| < 2.5$ ,  $\cancel{E}_T > 120$  GeV. We have studied the following SM background channels to estimate the efficiency of our analysis in this signal region:  $t\bar{t}$ +jets,  $t$ +jets,  $V$ +jets,  $h_{\text{SM}}$ +jets and QCD jets, where  $V$  represents the W and Z bosons.

The large  $\cancel{E}_T$  is expected to be balanced by the sole  $b$ -jet  $p_T$ . We can use this property of the signal events to isolate them from the background. There can be additional radiation jets in the signal but they are likely to have much smaller transverse momenta, while most of the background channels appear with additional jets produced from decays of heavier particles like the top quark or a gauge boson. These jets are, therefore, expected to have harder  $p_T$  distribution compared to the light jets in our signal. This can be another discriminatory factor. Top quark production channels pose a particular challenge to this signal region due to the large cross-section associated with them. However, the  $\cancel{E}_T$  distribution is likely to differ from the signal subjected to the choice of  $m_H$  and  $m_\chi$ . Moreover, the angular separation between the jet transverse momenta and the  $\cancel{E}_T$  in the signal are expected to be larger compared to that in the top quark production channels given the difference in decay topologies. Event shape analysis variables like transverse sphericity [45, 46] may also prove to be useful in this regard. The angular separation variables are also effective in reducing the potentially large contribution to the background originating from QCD multi-jet

production modes. All these considerations lead us to choose the following kinematic variables to be used in our multivariate analysis.

1. Number of light jets,  $N_j$ .
2. Transverse momentum of the b-jet,  $p_T^b$ .
3. Transverse momentum of the hardest light jet,  $p_T^{j1}$ .
4. Transverse momentum of the second hardest light jet,  $p_T^{j2}$ .
5. Missing transverse energy,  $\cancel{E}_T$ .
6. Angular separation between  $\cancel{E}_T$  and hardest light jet,  $\Delta\phi(\vec{E}_T, \vec{p}_T^{j1})$ .
7. Angular separation between  $\cancel{E}_T$  and second hardest light jet,  $\Delta\phi(\vec{E}_T, \vec{p}_T^{j2})$ .
8. Angular separation between  $\cancel{E}_T$  and the lone b-jet,  $\Delta\phi(\vec{E}_T, \vec{p}_T^b)$ .
9. Separation between the b-jet and hardest light jet,  $\Delta R(b, j1)$ .
10. Separation between the b-jet and second hardest light jet,  $\Delta R(b, j2)$ .
11. Effective mass,  $M_{EFF}$ .
12. Transverse sphericity,  $S_T = \frac{2\lambda_2}{\lambda_1 + \lambda_2}$ , where,  $\lambda_1$  and  $\lambda_2$  are the eigenvalues of the matrix

$$\frac{1}{\sum_i p_{Ti}} \sum_i \begin{pmatrix} p_{xi}^2 & p_{xi}p_{yi} \\ p_{yi}p_{xi} & p_{yi}^2 \end{pmatrix}.$$

### Signal Region 2: 3 b-jet

$H$  may also decay into a pair of  $b$  quark resulting in a 3  $b$ -jet final state with no direct source of missing energy. We put the following criteria to select events in this signal region: the final state should have three  $b$ -jet with a transverse momentum threshold of 25 GeV, while the hardest two  $b$ -jets must have  $p_T^b > 80$  GeV, no charged leptons be used in our multivariate analysis. with  $p_T^\ell > 10$  GeV. The  $|\eta|$  criteria remain same as in SR1. The dominant SM backgrounds studied for this signal region are:  $t\bar{t}$ +jets,  $t$ +jets,  $V$ +jets,  $VV$ +jets,  $bh_{SM}$ ,  $Zh_{SM}$  and QCD jets.

Lack of any direct source of missing energy in this signal region is a disadvantage against the background channels like  $V$  + jets and QCD multi-jet production channels. On the other hand, it can be a discriminating factor against background channels with large  $\cancel{E}_T$ , like  $t\bar{t}$ +jets. Among the three  $b$ -jets in the final state, a pair is generated from  $H$  decay. This can be used to reconstruct  $m_H$  to certain degree of accuracy and a window of invariant mass of this  $b$ -jet pair can be used as a discriminating variable. This  $b$ -jet pair is also likely to be well separated from the third  $b$ -jet. We choose the following list of kinematic variables to be used in our multivariate analysis to exploit these features.

1. Number of b-jets,  $N_b$ .
2. Number of light jets,  $N_j$ .
3. Transverse momentum of the hardest b-jet,  $p_T^{b1}$ .

4. Transverse momentum of the second hardest b-jet,  $p_T^{b2}$ .
5. Transverse momentum of the third hardest b-jet,  $p_T^{b3}$ .
6. Missing transverse energy,  $\cancel{E}_T$ .
7. Angular separation between  $\cancel{E}_T$  and hardest b-jet,  $\Delta\phi(\vec{E}_T, \vec{p}_T^{b1})$ .
8. Angular separation between  $\cancel{E}_T$  and second hardest b-jet,  $\Delta\phi(\vec{E}_T, \vec{p}_T^{b2})$ .
9. Angular separation between  $\cancel{E}_T$  and third hardest b-jet,  $\Delta\phi(\vec{E}_T, \vec{p}_T^{b3})$ .
10. Separation between two hardest b-jets,  $\Delta R(b1, b2)$ .
11. Invariant mass of hardest two b-jets,  $m_{inv}^{bb}$ .
12. Angular separation between the two hardest b-jet pair system and the third b-jet,  $\Delta\phi(\vec{p}_T^{bb}, \vec{p}_T^{b3})$ .
13. Sum of against momentum of hardest three b-jets,  $H_T^b$ .
14. Transverse sphericity,  $S_T$ .

### III.1. Results

For 1 b-jet +  $\cancel{E}_T$  final state, the most important kinematic variables are  $\cancel{E}_T$ ,  $\Delta R(b, j1)$ ,  $\Delta R(b, j2)$ ,  $\Delta\phi(\vec{E}_T, \vec{p}_T^b)$ ,  $p_T^b$  and  $M_{EFF}$ . The  $p_T$  of the light jets are also essential in obtaining the resultant sensitivity.  $N_j$ ,  $\Delta\phi(\vec{E}_T, \vec{p}_T^{j1, j2})$  and  $S_T$  do not have significant impact on the results. For 3 b-jet final state, the most important kinematic variables are  $\cancel{E}_T$ ,  $H_T^b$ ,  $m_{inv}^{bb}$ ,  $\Delta R(b1, b2)$  and  $S_T$ , whereas  $p_T^{b1}$ ,  $p_T^{b3}$  and  $\Delta\phi(\vec{p}_T^{bb}, \vec{p}_T^{b3})$  are also essential to obtain the best possible sensitivity. The other kinematic variables, namely  $N_j$  and  $\Delta\phi(\vec{E}_T, \vec{p}_T^{b1, b2, b3})$ , do not have significant impact on the results.

In order to showcase the sensitivity of our multivariate analysis, we choose some sample benchmark points with varied  $m_H$  and  $m_\chi$ . The  $H$  is assumed to decay with 50% branching ratio into each of the two available decay modes  $\chi\chi$  and  $b\bar{b}$ . In order to assess the most optimistic scenario, the value of the Wilson coefficient is kept fixed at its perturbative limit,  $\sqrt{4\pi} \sim 3.5$  and the  $H$ - $b\bar{b}$  coupling is computed such that  $H$  can decay with the above mentioned branching ratios. The area under the Receiver Operating Characteristic (ROC) curve (AUC) is a good estimator of the efficiency of the BDT classifier in identifying the signal and background events. The AUC numbers corresponding to all the benchmark points along with the required integrated luminosity to obtain a  $3\sigma$  statistical significance (and the corresponding  $5\sigma$  numbers within parentheses) are quoted in Table I for the energy scale  $\Lambda = 3$  TeV. The signal significance is calculated by  $\mathcal{S} = \frac{S}{\sqrt{S+B}}$ , where,  $S$  and  $B$  represents the number of signal and background events respectively.

Evidently, with  $\Lambda = 3$  TeV, one can probe a large portion of the parameter space. One can easily have a  $3\sigma$  evidence for  $m_H$  up to 2 TeV, and discovery  $\sim 1.5$  TeV for both  $m_\chi = 100$  GeV and 500 GeV through SR1. SR2 performs at par with SR1 or even better when  $m_H$  is



Benchmark Points	SR1(1 b-jet + $\cancel{E}_T$ )		SR2(3 b-jet)	
	AUC	Required Luminosity (fb $^{-1}$ )	AUC	Required Luminosity (fb $^{-1}$ )
BP1 ( $m_H = 600$ GeV, $m_\chi = 100$ GeV)	0.91	100.6 (279.4)	0.94	67.0 (186.0)
BP2 ( $m_H = 1400$ GeV, $m_\chi = 100$ GeV)	0.94	950.9 (2641.3)	0.88	1836.7 (5102.0)
BP3 ( $m_H = 1200$ GeV, $m_\chi = 500$ GeV)	0.94	578.7 (1607.6)	0.92	656.3 (1823.0)
BP4 ( $m_H = 1800$ GeV, $m_\chi = 500$ GeV)	0.95	2123.3 (5898.1)	0.86	7694.7 (> 10000)

TABLE I. Results of our BDT analysis performed using the XGBoost toolkit corresponding to four sample benchmark points for both the signal regions. For all these benchmark points,  $\Lambda = 3$  TeV and  $\text{BR}(H \rightarrow \chi\chi) = \text{BR}(H \rightarrow b\bar{b}) = 50\%$ . The Wilson coefficient  $f$  is kept fixed at its largest perturbative limit  $\sqrt{4\pi} \sim 3.5$ . The luminosity column shows the required luminosity to obtain  $3\sigma$  ( $5\sigma$ ) statistical significance.

on the lighter side. As the mass gap between  $m_H$  and  $m_\chi$  increases, SR1 performs better. This is mostly due to the presence of a large  $\cancel{E}_T$  in SR1. Clearly, a definite discovery significance of  $5\sigma$  can be attained for BP1, BP2 and BP3 through SR1 and BP1 and BP3 through SR2. We observed that in order to produce  $\text{BR}(H \rightarrow \chi\chi) = \text{BR}(H \rightarrow b\bar{b}) = 50\%$  with a  $H\text{-}\chi\text{-}\chi$  coupling  $\sim 1$ , one requires the  $H\text{-}b\text{-}\bar{b}$  coupling to be  $\sim 10^{-3}\text{-}10^{-4} \times y_{b\bar{b}h}|_{SM}$  for the benchmark points. This renders the production cross-section  $\sigma(pp \rightarrow bH)$  solely reliant on the dimension-6 operator, since the contribution from the s-channel mediated diagram in Fig. 1 is negligibly small in comparison.

The cross-section drops rapidly with increasing  $\Lambda$  and drops by one order of magnitude when increased from 3 TeV to 5 TeV. In Fig. 2 we show how much the sensitivity can change with the variation of the new physics scale. The y-axis shows the expected signal significance in both SR1 and SR2 for the highest possible luminosity of  $3000 \text{ fb}^{-1}$  at 14 TeV LHC. The x-axis shows variation of  $\Lambda$ . We show the results for BP1 and BP4 since these are the lightest and heaviest benchmark points respectively. Clearly, for BP1 at  $\Lambda = 5$  TeV, one can barely obtain a  $3\sigma$  statistical significance in SR2 and  $2\sigma$  in SR1. The trend reverses as the benchmark points become heavier. Now SR1 is the more sensitive one. However, for  $\Lambda = 5$  TeV, BP4 as well as BP2 and BP3 has poor sensitivity in either of the signal regions. We checked that even BP2 can barely achieve a signal significance of  $1\sigma$  in that case.

#### Comparison to cut-based analysis

In comparison to the multivariate analysis, a canonical cut-based analysis performs poorly. To illustrate this fact, we implemented a set of cuts carefully designed to maximize the efficiency in both the signal regions. For SR1, we demand that the final state must have only one  $b$ -jet with  $p_T^b > 250$  GeV, at least two light jets with  $p_T^j < 50$  GeV, no charged leptons,  $\cancel{E}_T > 250$  GeV,

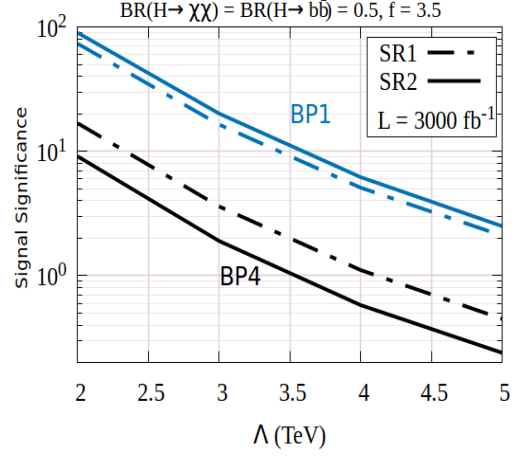


FIG. 2. The HL-LHC reach in signal significance in the two signal regions, SR1 (dashed line) and SR2 (solid line) as a function of  $\Lambda$  for BP1 (blue line) and BP4 (black line). The other two benchmark points lie in between.

$\Delta\phi(\vec{\cancel{E}}_T, \vec{p}_T^b) > 1.0$ ,  $M_{EFF} > 500$  GeV and  $S_T < 0.1$ . For SR2, the final state must have at least three  $b$ -jets with the hardest two having  $p_T^b > 150$  GeV, no charged leptons, no light jets with  $p_T^j > 50$  GeV,  $\cancel{E}_T < 100$  GeV,  $|m_{inv}^{bb} - 125.0| > 25$  GeV,  $H_T^b > 500$  GeV,  $\Delta\phi(\vec{p}_T^{bb}, \vec{p}_T^{b3}) > 1.0$  and  $S_T > 0.1$ . With these set of cuts, we inspect the four benchmark points and the aforementioned background channels. The results are presented in Table II. We observed that through such a cut-based analysis, for BP1 one can attain a  $3\sigma$  ( $5\sigma$ ) signal significance at an integrated luminosity of  $214.2$  ( $595.1$ )  $\text{fb}^{-1}$  and  $500.1$  ( $1389.2$ )  $\text{fb}^{-1}$  in SR1 and SR2, respectively. BP3 can only be probed in SR1 close to a signal significance of  $3\sigma$ . BP3 cannot be probed in SR2 within the luminosity reach. BP2 and BP4 remain completely out of reach in both the signal regions. Thus, it is evident that the multivariate BDT analysis offers a distinct advantage over the cut-based analysis. Note that, for the chosen set of optimized cuts SR1 always has better sensitivity compared to SR2. This is in contrast to our multivariate analysis results which clearly show that the relative sensitivity is reversed for BP1. It turns out that SR2 is more effective within a small parameter space highlighting the fact that the BDT algorithm is more sensitive to the subtle changes in kinematics in order to identify the signal events. This feature is discussed in more detail in the subsequent section.

#### III.2. Discovery reach at HL-LHC

We now proceed to assess the extent to which the 14 TeV LHC can probe the present scenario at the highest possible projected luminosity,  $3000 \text{ fb}^{-1}$ . For this, we study two sample values of  $m_\chi = 100$  and  $500$  GeV. Fig. 3 shows the required  $\sigma(pp \rightarrow bH) \times \text{BR}(H \rightarrow \chi\chi)$  and

Benchmark Points	Required Luminosity (fb <sup>-1</sup> )	
	SR1(1 b-jet + $\cancel{E}_T$ )	SR2(3 b-jet)
BP1	214.2	500.1
BP2	9305.1	>10000
BP3	3748.4	>10000
BP4	>10000	>10000

TABLE II. Results of cut-based analysis for the four sample benchmark points for both the signal regions. For all these benchmark points,  $\Lambda = 3$  TeV and  $\text{BR}(H \rightarrow \chi\chi) = \text{BR}(H \rightarrow b\bar{b}) = 50\%$ . The Wilson coefficient  $f$  is kept fixed at its largest perturbative limit  $\sqrt{4\pi} \sim 3.5$ . The luminosity column shows the required luminosity to obtain  $3\sigma$  statistical significance.

$\sigma(pp \rightarrow bH) \times \text{BR}(H \rightarrow b\bar{b})$  as a function of  $m_H$  for SR1 and SR2, respectively, such that a  $3\sigma$  statistical significance is obtained at  $3000 \text{ fb}^{-1}$ . The  $m_H$  threshold is chosen such that  $H \rightarrow \chi\chi$  decay mode is open. Understandably, one can obtain non-zero event rate for SR2 even below this  $m_H$  threshold. One can simply look at the existing experimental studies looking for non-standard Higgs bosons decaying into a pair of  $b$ -quarks for such limits, see e.g. [47]. For both  $m_\chi = 100$  GeV and 500 GeV, the trend looks same. At the low  $m_H$  region as well as high  $m_H$  region, SR1 has better sensitivity compared to SR2 which is only more efficient within an intermediate range. In the low  $m_H$  region, kinematics of the final state  $b$ -quarks are not distinctly different from their SM counterpart in SR2. Expectedly, the situation improves dramatically with increasing  $m_H$  before the sensitivity saturates. On the other hand, SR1 is always associated with a large  $\cancel{E}_T$  which helps it gain better sensitivity specially in the low  $m_H$  region.  $\cancel{E}_T$  along with the angular variables only get more and more distinctive with increasing  $m_H$ , making SR1 the more sensitive channel at heavier mass region as well. The sensitivity in the 1-2 TeV range of  $m_H$  is very similar for both the two different choices of  $m_\chi$  indicating the fact that mass of the invisible particle does not have a severe impact on the outcome. It should be noted that the results in Fig. 3 depend on  $m_H$  only. Whatever choice of  $\Lambda$  predicts a particular  $\sigma(pp \rightarrow bH) \times \text{BR}(H \rightarrow XX)$  for each  $m_H$  is similarly favourable, so long as the Lorentz structure of the effective interaction is the same, since the latter has a role in deciding the efficiency of the BDT analysis.

It is worth mentioning that the experimental collaborations are yet to probe the signal region SR1 in the context of heavy scalar search. However, they have studied the multi  $b$ -jet final state SR2 [13, 14] as mentioned before. These studies combine the four and five flavor contributions to the cross-section of a signal consisting of at least three  $b$ -jets and present their exclusion limit on  $\sigma(pp \rightarrow b\bar{b}H) \times \text{BR}(H \rightarrow b\bar{b})$  as a function of  $m_H$  with  $\sqrt{s} = 13$  TeV for an integrated luminosity  $35.7 \text{ fb}^{-1}$  [13] and  $27.8 \text{ fb}^{-1}$  [14]. In the context of this work,  $\sigma(pp \rightarrow b\bar{b}H) \times \text{BR}(H \rightarrow b\bar{b})$  is negligibly small by virtue of a small  $Hb\bar{b}$  coupling as discussed in section II. However, one would expect a similar exclusion limit for

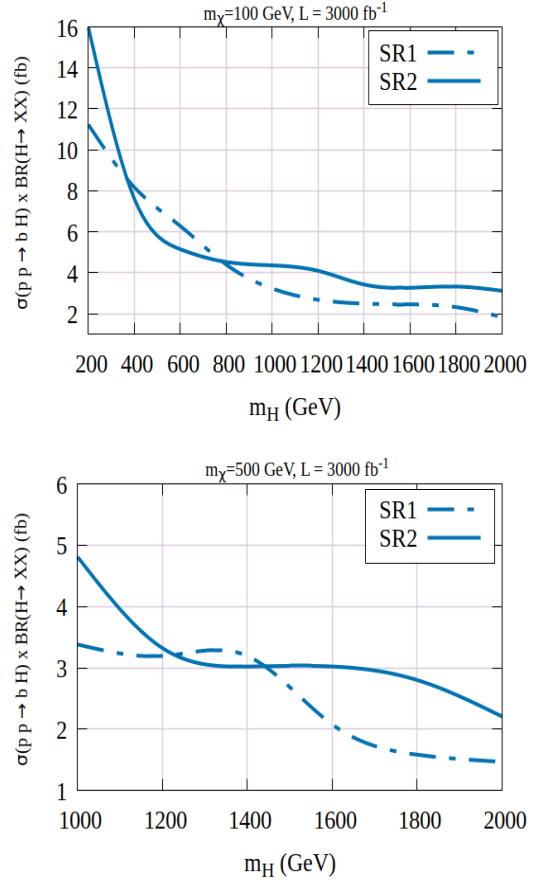


FIG. 3. The HL-LHC reach in  $\sigma(pp \rightarrow bH) \times \text{BR}(H \rightarrow XX)$ , where  $XX \equiv \chi\chi$  for SR1 (dashed line) and  $b\bar{b}$  for SR2 (solid line) as a function of the heavy scalar mass,  $m_H$ , in order to achieve a  $3\sigma$  statistical significance. The results are obtained through our BDT analyses performed using the XGBoost toolkit.

$\sigma(pp \rightarrow bH) \times \text{BR}(H \rightarrow b\bar{b})$  as well. Even if we assume in a conservative way, that both these exclusion limits lie in the same ballpark, our benchmark points still cannot be excluded with the present experimental sensitivity. Moreover, we present in Fig. 3 the highest possible sensitivity that can be reached at the LHC in order to attain a  $3\sigma$  statistical significance. The required  $\sigma(pp \rightarrow bH) \times \text{BR}(H \rightarrow b\bar{b})$  in this figure over a wide range of  $m_H$  lies at least one order of magnitude below the present experimental sensitivity presented in [13, 14].

We use the results presented in Fig. 3 to ascertain the required values of the Wilson coefficient,  $f$ , that can produce the projected  $\sigma(pp \rightarrow bH) \times \text{BR}(H \rightarrow XX)$ . While doing so, we take note of the fact that there are two competing production channels. As a result, the choice of  $Hb\bar{b}$  vertex factor plays a crucial role. Since our goal is to determine the accessible range of  $f$ , we choose a parameter space such that the  $Hb\bar{b}g$  effective vertex diagram contributes dominantly to the cross-section. Therefore, we keep the  $Hb\bar{b}$  vertex factor,  $V_{Hb\bar{b}} = c \times y_{b\bar{b}h}|_{SM}$

small. Here  $h$  is the 125 GeV Higgs boson and  $c$  is just a scale factor. We keep  $c = 10^{-4}$  to keep this coupling sufficiently small. In order to ascertain the maximum impact of our analysis, we keep  $\text{BR}(H \rightarrow \chi\chi) = 1.0$  and  $\text{BR}(H \rightarrow b\bar{b}) = 1.0$  for SR1 and SR2 respectively. The results are shown in Fig. 4 for  $m_\chi = 100$  GeV and  $\Lambda = 3$  and 5 TeV. The upper limit of  $f$  is restricted to

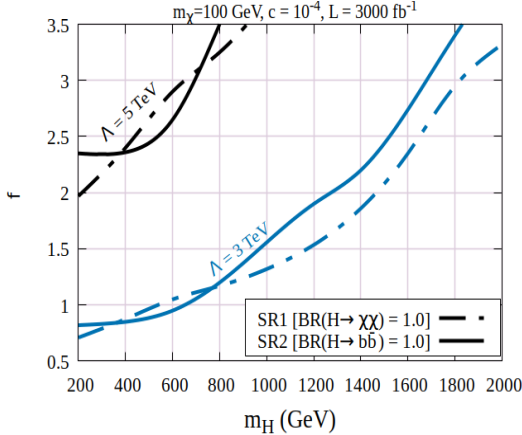


FIG. 4. The distribution of the Wilson coefficient,  $f$  as a function of  $m_H$  for SR1 (dashed line) and SR2 (solid line) in order to produce the required  $\sigma(pp \rightarrow bH) \times \text{BR}(H \rightarrow XX)$  resulting in a  $3\sigma$  statistical significance at HL-LHC for  $m_\chi = 100$  GeV,  $c = 10^{-4}$ .  $\text{BR}(H \rightarrow \chi\chi) = \text{BR}(H \rightarrow b\bar{b}) = 1.0$  respectively for SR1 and SR2. The results are shown for  $\Lambda = 3$  TeV (blue line) and 5 TeV (black line).

the perturbative limit. The coupling strength of  $H$  to the pair of invisible particles  $V_{H\chi\chi}$  is fixed within its perturbative limit such that the criteria on the two relevant branching ratios are met. Clearly, SR1 has a greater sensitivity compared to SR2 apart from a small part of the parameter region as also seen in Fig. 3. For  $\Lambda = 3$  TeV, heavy higgs mass of  $\sim 2$  TeV can be easily probed at the HL-LHC up to a signal significance of  $3\sigma$ . The Wilson coefficient,  $f$  can be probed all the way down to  $\sim 0.6$ . The sensitivity worsens understandably with increasing  $\Lambda$  and as evident, one can only probe  $m_H \lesssim 1$  TeV and  $f \gtrsim 1.9$ . Note that, for a large enough  $c \gtrsim 10^{-2}$ , the production cross-section will be dominated by the s-channel  $b$ -quark mediated diagram. In that case, SR2 will be the favoured signal region to probe the scenario throughout the parameter space. However, that does not improve the sensitivity in probing smaller values of  $f$  unless the  $Hb\bar{b}$  coupling is measured to a high degree of precision such that one can discern the comparatively much smaller contribution to the event rate arising from the dimension six operator. Here we discussed the  $m_\chi = 100$  GeV case as an example to showcase the extent of the sensitivity of our multivariate analysis. The accessible range of  $f$  can be quite different for other choices of  $m_\chi$ .

#### IV. SUMMARY AND CONCLUSION

In this work we have explored two signal regions through multivariate analysis to probe the prospect of a heavy scalar being singly produced in association with a  $b$ -quark at the 14 TeV LHC. The production channel  $bg \rightarrow bH$  can get contribution from an effective interaction of the form  $Hb\bar{b}g$ . Such an interaction can be generated from viable dimension six operators. However, one needs to treat the  $b$ -quarks as partons in order for this interaction to contribute to the cross-section starting from a proton-proton collision. Instead of exploring some specific new physics model we parameterize its effect through the interaction strength and ascertain the sensitivity of the LHC to probe this scenario at its peak projected luminosity. In order to do so, we identify the most probable visible decay mode of  $H$  along with an invisible decay mode to construct two signal regions. Looking at the kinematics of the final states we choose two sets of kinematic variables to carry out our multivariate analysis using the XGBoost toolkit. We show that even though the signal regions have potentially large SM backgrounds, one can still achieve good sensitivity through this kind of multivariate analysis. We determine the required signal cross-sections in order to obtain  $3\sigma$  statistical significance at the 14 TeV LHC with an integrated luminosity of  $3000 \text{ fb}^{-1}$ . We present the result as function of  $m_H$ , which is model independent and is applicable to any new physics model giving rise to similar interactions. We further use this information to determine the efficiency of the LHC in probing the Wilson coefficient  $f$  of the effective interaction. We find that  $m_H \lesssim 2$  TeV can easily be probed with a  $3\sigma$  statistical significance staying within the perturbative limit of  $f$  with the new physics scale set at 3 TeV. The situation worsens considerably with  $\Lambda = 5$  TeV, the reach in  $m_H$  being restricted to below the TeV range. The probe on  $f$  is dependent on the choice of  $Hb\bar{b}$  interaction strength. Our focus being the new effective interaction, we keep the  $Hb\bar{b}$  coupling strength to be small. We observe that  $f < 0.5$  is difficult to probe in either of the two signal regions. The results also show that in presence of such an effective interaction one can in principle probe much smaller  $Hb\bar{b}$  coupling compared to the existing experimental studies.

#### V. ACKNOWLEDGEMENTS

BM acknowledges the hospitality of Katri Huitu and the Helsinki institute of Physics during the early part of the project. The research of BM till November, 2019, was supported by the Department of Atomic Energy, Government of India, through funding made available to the Regional Centre for Accelerator-based Particle Physics, Harish-Chandra Research Institute, Allahabad.

- 
- [1] M. Aaboud *et al.* [ATLAS Collaboration], JHEP **1901**, 030 (2019) doi:10.1007/JHEP01(2019)030 [arXiv:1804.06174 [hep-ex]].
- [2] A. M. Sirunyan *et al.* [CMS Collaboration], JHEP **1808**, 152 (2018) doi:10.1007/JHEP08(2018)152 [arXiv:1806.03548 [hep-ex]].
- [3] A. M. Sirunyan *et al.* [CMS Collaboration], JHEP **1901**, 040 (2019) doi:10.1007/JHEP01(2019)040 [arXiv:1808.01473 [hep-ex]].
- [4] A. M. Sirunyan *et al.* [CMS Collaboration], Phys. Lett. B **788**, 7 (2019) doi:10.1016/j.physletb.2018.10.056 [arXiv:1806.00408 [hep-ex]].
- [5] M. Aaboud *et al.* [ATLAS Collaboration], JHEP **1811**, 040 (2018) doi:10.1007/JHEP11(2018)040 [arXiv:1807.04873 [hep-ex]].
- [6] M. Aaboud *et al.* [ATLAS Collaboration], Phys. Rev. Lett. **121**, no. 19, 191801 (2018) Erratum: [Phys. Rev. Lett. **122**, no. 8, 089901 (2019)] doi:10.1103/PhysRevLett.122.089901, 10.1103/PhysRevLett.121.191801 [arXiv:1808.00336 [hep-ex]].
- [7] G. Aad *et al.* [ATLAS Collaboration], Phys. Lett. B **801**, 135145 (2020) doi:10.1016/j.physletb.2019.135145 [arXiv:1908.06765 [hep-ex]].
- [8] M. Aaboud *et al.* [ATLAS Collaboration], Phys. Lett. B **793**, 499 (2019) doi:10.1016/j.physletb.2019.04.024 [arXiv:1809.06682 [hep-ex]].
- [9] D. Chowdhury and O. Eberhardt, JHEP **1805**, 161 (2018) doi:10.1007/JHEP05(2018)161 [arXiv:1711.02095 [hep-ph]].
- [10] W. Buchmuller and D. Wyler, Nucl. Phys. B **268**, 621 (1986). doi:10.1016/0550-3213(86)90262-2
- [11] B. Grzadkowski, M. Iskrzynski, M. Misiak and J. Rosiek, JHEP **1010**, 085 (2010) doi:10.1007/JHEP10(2010)085 [arXiv:1008.4884 [hep-ph]].
- [12] A. Dedes, W. Materkowska, M. Paraskevas, J. Rosiek and K. Suxho, JHEP **1706**, 143 (2017) doi:10.1007/JHEP06(2017)143 [arXiv:1704.03888 [hep-ph]].
- [13] A. M. Sirunyan *et al.* [CMS Collaboration], JHEP **1808**, 113 (2018) doi:10.1007/JHEP08(2018)113 [arXiv:1805.12191 [hep-ex]].
- [14] G. Aad *et al.* [ATLAS Collaboration], arXiv:1907.02749 [hep-ex].
- [15] R. Harlander, M. Kramer and M. Schumacher, arXiv:1112.3478 [hep-ph].
- [16] G. C. Branco, P. M. Ferreira, L. Lavoura, M. N. Rebelo, M. Sher and J. P. Silva, Phys. Rept. **516**, 1 (2012) doi:10.1016/j.physrep.2012.02.002 [arXiv:1106.0034 [hep-ph]].
- [17] S. Forte, D. Napoletano and M. Ubiali, Phys. Lett. B **751**, 331-337 (2015) doi:10.1016/j.physletb.2015.10.051 [arXiv:1508.01529 [hep-ph]].
- [18] M. Bonvini, A. S. Papanastasiou and F. J. Tackmann, JHEP **11**, 196 (2015) doi:10.1007/JHEP11(2015)196 [arXiv:1508.03288 [hep-ph]].
- [19] M. Bonvini, A. S. Papanastasiou and F. J. Tackmann, JHEP **10**, 053 (2016) doi:10.1007/JHEP10(2016)053 [arXiv:1605.01733 [hep-ph]].
- [20] S. Forte, D. Napoletano and M. Ubiali, Phys. Lett. B **763**, 190-196 (2016) doi:10.1016/j.physletb.2016.10.040 [arXiv:1607.00389 [hep-ph]].
- [21] C. Duhr, F. Dulat, V. Hirschi and B. Mistlberger, [arXiv:2004.04752 [hep-ph]].
- [22] G. Cacciapaglia, A. Carvalho, A. Deandrea, T. Flacke, B. Fuks, D. Majumder, L. Panizzi and H. S. Shao, Phys. Lett. B **793**, 206 (2019) doi:10.1016/j.physletb.2019.04.056 [arXiv:1811.05055 [hep-ph]].
- [23] C. Arnesen, I. Z. Rothstein and J. Zupan, Phys. Rev. Lett. **103**, 151801 (2009) doi:10.1103/PhysRevLett.103.151801 [arXiv:0809.1429 [hep-ph]].
- [24] P. C. Bhat, Ann. Rev. Nucl. Part. Sci. **61**, 281-309 (2011) doi:10.1146/annurev.nucl.012809.104427
- [25] Breiman, Leo, Joseph H Friedman, R. A. Olshen and C. J. Stone, "Classification and Regression Trees." (Wadsworth International Group, Belmont, 1984).
- [26] Freund, Y, Schapire, R. E, "A decision-theoretic generalization of on-line learning and an application to boosting", J. Comput. Syst. Sci. **55**, 119-139 (1997)
- [27] B. P. Roe, H. J. Yang, J. Zhu, Y. Liu, I. Stancu and G. McGregor, Nucl. Instrum. Meth. A **543**, no.2-3, 577-584 (2005) doi:10.1016/j.nima.2004.12.018 [arXiv:physics/0408124 [physics]].
- [28] G. Aad *et al.* [ATLAS], Phys. Lett. B **716**, 1-29 (2012) doi:10.1016/j.physletb.2012.08.020 [arXiv:1207.7214 [hep-ex]].
- [29] S. Chatrchyan *et al.* [CMS], Phys. Lett. B **716**, 30-61 (2012) doi:10.1016/j.physletb.2012.08.021 [arXiv:1207.7235 [hep-ex]].
- [30] P. Baldi, P. Sadowski and D. Whiteson, Nature Commun. **5**, 4308 (2014) doi:10.1038/ncomms5308 [arXiv:1402.4735 [hep-ph]].
- [31] T. Chen and C. Guestrin, doi:10.1145/2939672.2939785 arXiv:1603.02754 [cs.LG].
- [32] J. Alwall, M. Herquet, F. Maltoni, O. Mattelaer and T. Stelzer, JHEP **1106**, 128 (2011) [arXiv:1106.0522 [hep-ph]].
- [33] J. Alwall *et al.*, JHEP **1407**, 079 (2014) [arXiv:1405.0301 [hep-ph]].
- [34] T. Sjostrand, S. Mrenna and P. Z. Skands, JHEP **0605**, 026 (2006) [hep-ph/0603175].
- [35] T. Sjostrand *et al.*, Comput. Phys. Commun. **191**, 159 (2015) [arXiv:1410.3012 [hep-ph]].
- [36] R. D. Ball *et al.*, Nucl. Phys. B **867**, 244 (2013) [arXiv:1207.1303 [hep-ph]].
- [37] R. D. Ball *et al.* [NNPDF Collaboration], JHEP **1504**, 040 (2015) [arXiv:1410.8849 [hep-ph]].
- [38] J. de Favereau *et al.* [DELPHES 3 Collaboration], JHEP **1402**, 057 (2014) [arXiv:1307.6346 [hep-ex]].
- [39] M. Selvaggi, J. Phys. Conf. Ser. **523**, 012033 (2014).
- [40] A. Mertens, J. Phys. Conf. Ser. **608**, no. 1, 012045 (2015).
- [41] M. Cacciari, G. P. Salam and G. Soyez, Eur. Phys. J. C **72**, 1896 (2012) [arXiv:1111.6097 [hep-ph]].
- [42] M. Cacciari, G. P. Salam and G. Soyez, JHEP **0804**, 063 (2008) [arXiv:0802.1189 [hep-ph]].
- [43] ATLAS Collaboration, ATL-PHYS-PUB-2015-022.
- [44] <https://cp3.irmp.ucl.ac.be/projects/madgraph/wiki/FAQ-General-13>
- [45] A. Banfi, G. P. Salam and G. Zanderighi, JHEP **0408**, 062 (2004) doi:10.1088/1126-6708/2004/08/062 [hep-ph/0407287].



- [46] B. Abelev *et al.* [ALICE Collaboration], Eur. Phys. J. C **72**, 2124 (2012) doi:10.1140/epjc/s10052-012-2124-9 [arXiv:1205.3963 [hep-ex]].
- [47] V. Khachatryan *et al.* [CMS Collaboration], JHEP **1511**, 071 (2015) doi:10.1007/JHEP11(2015)071 [arXiv:1506.08329 [hep-ex]].